Chinese Chemical Letters 33 (2022) 4798–4802

Contents lists available at ScienceDirect

Chinese Chemical Letters

journal homepage: www.elsevier.com/locate/cclet

High sensitivity ratiometric fluorescence temperature sensing using the microencapsulation of $CsPbBr_3$ and $K_2SiF_6:Mn^{4+}$ phosphor

Jingwen Jin[a], Jie Lin[a], Yipeng Huang[a], Linchun Zhang[a], Yaqi Jiang[a], Dongjie Tian[a], Fangyuan Lin[a], Yiru Wang[a], Xi Chen[a,b,c,*]

[a] Department of Chemistry and the MOE Key Laboratory of Spectrochemical Analysis & Instrumentation, College of Chemistry and Chemical Engineering, Xiamen University, Xiamen 361005, China
[b] State Key Laboratory of Marine Environmental Science, Xiamen University, Xiamen 361005, China
[c] Shenzhen Research Institute of Xiamen University, Shenzhen 518000, China

ARTICLE INFO

Article history:
Received 28 October 2021
Revised 1 December 2021
Accepted 7 January 2022
Available online 14 January 2022

Keywords:
Ratiometric fluorescence sensing
High sensitivity
Perovskite nanocrystals
Temperature
Microencapsulation

ABSTRACT

A dual emission sensing film has been prepared for colorimetric temperature sensing using $CsPbBr_3$ perovskite nanocrystals ($CsPbBr_3$ NCs) and manganese doped potassium fluorosilicate ($K_2SiF_6:Mn^{4+}$, KSF) encapsulated in polystyrene by a microencapsulation strategy. The $CsPbBr_3$-KSF-PS film shows good temperature sensing response from 30 °C to 70 °C, with a relative temperature sensitivity (S_r) up to 10.31% $°C^{-1}$ at 45 °C. Meanwhile, the film maintains more than 95% intensity after 6 heating-cooling cycles and keeps its fluorescence characteristics after 3 months. The film can be used to monitor temperature change by naked eye under a UV lamp. In particular, the temperature discoloration point of the sensing film can be controlled by the ratio change of $CsPbBr_3$:KSF to expand its applications. The study of the $CsPbBr_3$-KSF-PS sensing mechanism in this work is helpful to provide effective strategies for the design of reliable, high sensitivity and stable temperature sensing system using $CsPbBr_3$ NCs.

As one of the earliest developed and most frequently used sensors, temperature sensors have been applied in scientific research, industrial and agricultural production, life medical care and diagnosis [1,2]. Currently, the mainstream temperature sensors include contact thermocouples and non-contact infrared modes. In particular, optical based non-contact thermometers have attracted immense intention [3] because of its characteristics of fast-response and real-time temperature sensing. At present, the optical temperature sensors have been developed by using various luminescent materials such as rare earth phosphors [4–7], metal-organic framework (MOF) [8], and quantum dots (QDs) [9]. However, the relative temperature sensitivity (S_r) of these thermal probes, which is the most critical parameter for evaluating the sensing performance of an optical thermometer, remains no more than 2% for per kelvin [10]. It is still necessary and urgent to develop feasible strategies or novel thermal probes for the sensitivity enhancement.

Several sensing modes such as fluorescence intensity [11], emission spectral shift [12], fluorescence lifetime [13] or fluorescence intensity ratio (FIR) [14,15] could be employed for optical sensors. Among them, FIR is a superior technique for the optical temperature sensing. Compared with the single-emission fluorescence probe, the double-emission mode has the advantages of high precision, high sensitivity and visualization due to its self-calibration and color changeable features [16], which is convenient for on-site sensing applications. Generally, the photoluminescence (PL) color change is easier to be recognized by human eyes than those based on the single emission intensity change, which is conducive to the practical application of visualization. Although there have been reports on the two-dimensional thermal imaging using a reversible colorimetric temperature nanosensor by encapsulating two color luminescence dyes [15,17], it is still unsatisfactory to accurately identify the color change of the luminescent composite materials with blue-emission since the human eyes are sensitive to red and green lights.

All-inorganic $CsPbX_3$ perovskite nanocrystals ($CsPbX_3$ NCs, X = Cl^-, Br^-, I^-) have attracted tremendous research interests in the fields of solar cells [18], light-emitting diodes (LEDs) [19], photoelectric detectors [20], temperature sensing [14,21], *etc.* Recently, because of their excellent optical properties, such as high photoluminescence quantum yield (PLQY, nearly 100%), narrow full width at half maximum (FWHM), high defect tolerance, tunable band gap throughout the visible spectrum by halogen

* Corresponding author.
E-mail address: xichen@xmu.edu.cn (X. Chen).

https://doi.org/10.1016/j.cclet.2022.01.017
1001-8417/

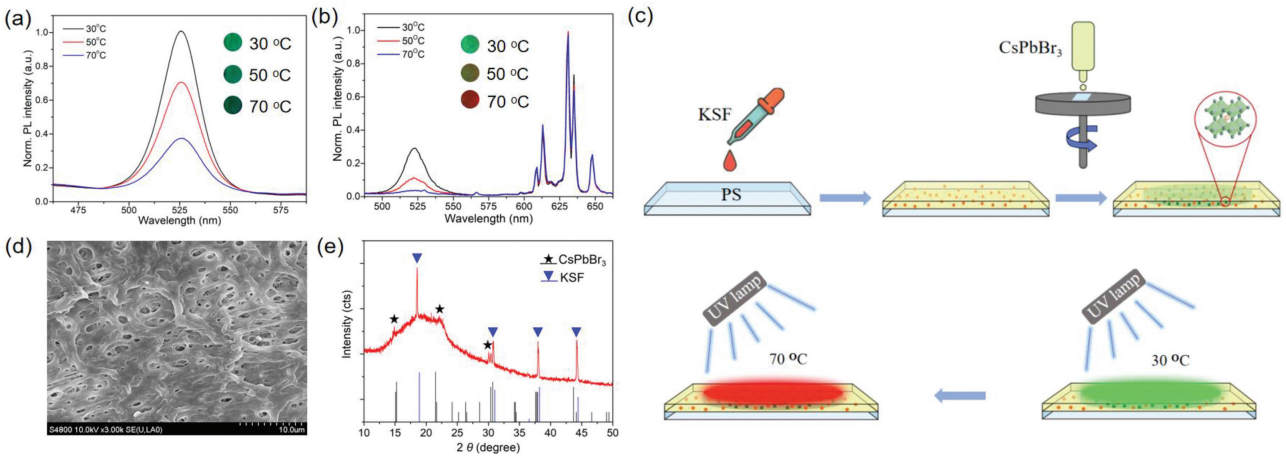

Fig. 1. (a) Fluorescence spectra of $CsPbBr_3$ films and (b) $CsPbBr_3$-KSF films at 30 °C, 50 °C and 70 °C. (c) Schematic diagram of *in-situ* grown $CsPbBr_3$-KSF-PS film synthesis. (d) SEM images of $CsPbBr_3$-KSF films. (e) XRD patterns of $CsPbBr_3$-KSF films, $CsPbBr_3$ NCs and KSF powder.

composition or dimension manipulation, *etc.* [22–24]. The green or red emitting emissive $CsPbX_3$ NCs can be easily synthesized for high-efficient colorimetric sensing using the emission-tunable property. In addition, the narrow FWHM of $CsPbX_3$ NCs is in favor of introducing additional phosphors for FIR sensing. In contrast with traditional quantum dots, $CsPbX_3$ perovskite NCs have extraordinary defect-tolerant properties [22]. Recently, several strategies for *in-situ* confined growth of ligand-free and highly stable $CsPbX_3$ NCs in mesoporous silicon templates [23,25], glass [26] or polymer matrix [27] have been developed. Generally, the preparation of mesoporous silica templates for the confined formation of $CsPbX_3$ NCs is time-consuming, and the synthesis of glass stabilized $CsPbX_3$ NCs should be operated at high temperature. In order to realize the facile synthesis, the simple and room temperature [28] *in-situ* growth of $CsPbX_3$ NCs in polymer matrix is suitable choice to construct an optical temperature sensing film with high stability.

Herein, $CsPbBr_3$ NCs with green emission were selected as the temperature responsive material, and K_2SiF_6 with bright red emission was selected as the reference material for the construction of FIR temperature sensing film. The as prepared film shows good stability and high sensitivity towards the temperature change.

As the report, $CsPbX_3$ NCs show a great linear relationship with the temperature change [29]. Compared with those of $CsPbX_3$ NCs, $CsPbBr_3$ NCs has a large quenching degree and the best thermal stability, which can provide durable green light with strong PL and high color purity. As an all-inorganic perovskite, the poor water resistance of $CsPbBr_3$ NCs greatly impedes their applications. In this work, $CsPbBr_3$ NCs are directly grown in the PS layer to form a uniform temperature sensing film. As shown in Fig. S1 (Supporting information), the *in-situ* grown $CsPbBr_3$ NCs presented obvious difference PL responses towards the temperature change, and a good linear relationship between the PL intensity and the temperature change could be found. Due to the dense PS film and its good hydrophobicity, $CsPbBr_3$ NCs are isolated from the external environment in the PS film, and the sensing film reveals excellent anti-water characteristics.

In the preparation of the temperature sensing film, KSF, a kind of commercialized phosphor used in LED industry, was selected as a reference probe since it is of high stable quality and giving bright red light with narrow half peak width (Fig. S1). In order to compare the sensing characteristics of the $CsPbBr_3$-KSF-PS film, a film without KSF was prepared using the same method. PL spectra of two films at 30 °C, 50 °C and 70 °C were collected under the same test conditions. As shown in Fig. 1b, the PL intensity of $CsPbBr_3$-PS film was decreased by 64% when the temperature increased from 30 °C to 70 °C. Comparatively, the $CsPbBr_3$-KSF-PS film presented greater quenching degree with the same temperature change (Fig. 1c). Under the excitation of 365 nm, the color changed from bright green to dark gradually for the $CsPbBr_3$-PS film with the temperature increase, while more significant color change from green to yellow and finally to red could be observed for the $CsPbBr_3$-KSF-PS film. Obviously, the addition of KSF into the $CsPbBr_3$-PS film resulted in higher sensitivity and color discrimination. Since the PL intensity of the introduced red-emitting KSF was basically unchanged during the temperature sensing, the thermal quenching of $CsPbBr_3$ caused its green PL intensity decrease. The combination of these two factors made a significant color change of the $CsPbBr_3$-KSF-PS film.

As illustrated in Fig. 1c, the $CsPbBr_3$-KSF-PS film was prepared using the swelling–deswelling microencapsulation strategy developed by Shin-Tson Wu *et al.* [25]. In this study, the KSF-PS film was fabricated prior to the *in-situ* growth of $CsPbBr_3$ NCs. Compared with the flat surface of pristine PS film, the surface of KSF-PS film shows apparent humped particles (Fig. S2 in Supporting information) due to the addition of KSF phosphors. After the spin-coating of $CsPbBr_3$ precursor solution on KSF-PS film, the solvent (DMF) causes the swelling of PS, then the $CsPbBr_3$ precursor solution penetrates into the PS. With the subsequent vacuum drying, the evaporation of DMF generates a myriad of nano-/micro-pores as shown in Fig. 1d, providing excellent templates for the *in-situ* space confinement of $CsPbBr_3$ NCs. The XRD pattern of $CsPbBr_3$-KSF-PS film shows the diffraction peaks at 15.081°, 21.498° and 30.378° belonging to the crystal plane of (001), (110) and (002) for the orthorhombic $CsPbBr_3$ (Fig. 1e) (black line, pentacle), while the existence of diffraction peaks of KSF (Fig. 1e) (blue line, triangle) further confirms the KSF phosphors has been embedded into the PS matrix. The result confirms the formation of $CsPbBr_3$ NCs in the film.

The as-prepared $CsPbBr_3$-KSF-PS film shows a PL peak of $CsPbBr_3$ NCs at 523 nm with a narrow half peak width (17 nm) and the PL peak of KSF centered at 631 nm (Fig. 2a). With the temperature increased from 30 °C to 70 °C, the KSF PL intensity kept constant almost. The PL intensity (I) remained over 95% of its original intensity (I_0) (Fig. S1). However, the PL intensity of $CsPbBr_3$ NCs at 523 nm emission substantially decreased by 86.9% under the same temperature increase process. Based on the fluorescence characteristics, a FIR mode could be constituted for self-calibration temperature sensing using $CsPbBr_3$ NCs and KSF phosphors. The PL intensity of $CsPbBr_3$ NCs as a temperature function can be

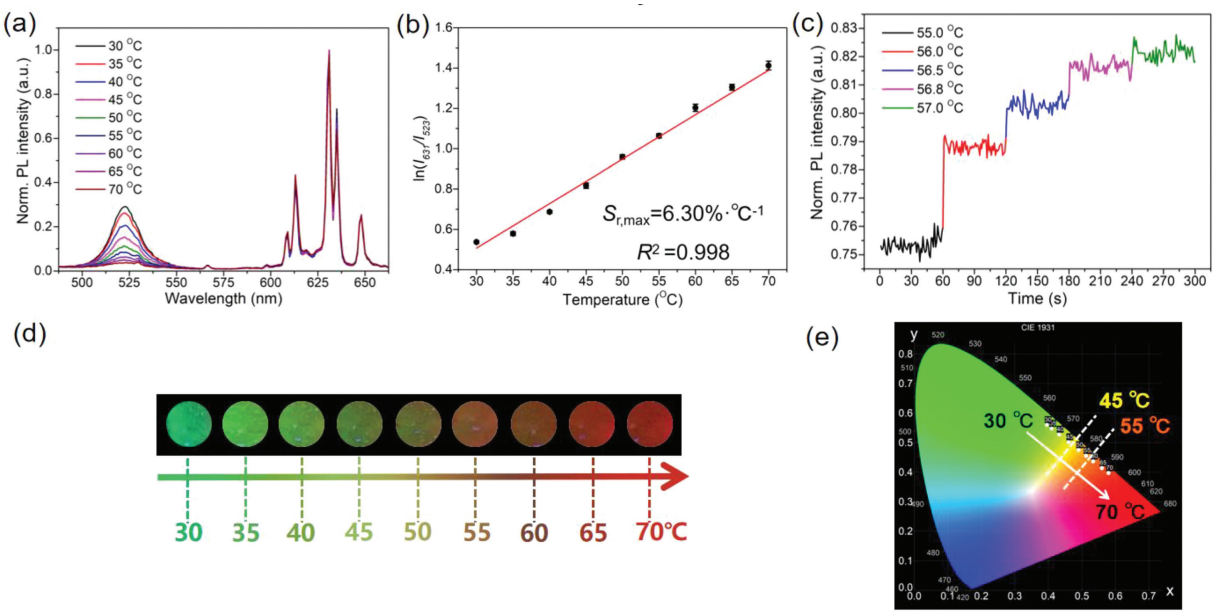

Fig. 2. (a) Fluorescence spectra of the film with different temperature. (b) The linear relationship between the logarithm of FIR and the temperature. (c) FIR-Time diagram at different temperatures. (d) The images of membrane under the excitation of 365 nm. (e) The color gamut map (CIE 1931) corresponding to the spectrum, the temperature discoloration points are 45 °C and 55 °C respectively.

described by the following equation (Eq. 1) [30]:

$$I(T) = \frac{I_0}{1 + A\exp^{-E_b/(k_B T)}} \quad (1)$$

where $I(T)$ and I_0 are the PL intensities at temperature T and temperature close to 0 K (in absolute temperature), respectively. A is a pre-exponential factor, k_B is the Boltzmann constant and E_b is the exciton binding energy. For the FIR system, the temperature-dependent FIR value can be described as follows (Eq. 2),

$$\mathrm{FIR} = \frac{I_{523}}{I_{631}} = B + C\exp\left(-\frac{\Delta E}{k_B T}\right) \quad (2)$$

where I_{523} and I_{631} are the emission intensities of the $CsPbBr_3$ NCs and KSF, respectively. B and C are constants determined by the intrinsic properties of the material, and ΔE is the thermal quenching activation energy for the $CsPbBr_3$-KSF film. Herein, as the temperature increases, the logarithm value of FIR for the $CsPbBr_3$-KSF-PS film shows a great linear relationship with the temperature (Fig. 2b), and the result can be well fitted by the equation: $y = 0.01742x - 0.2046$ (x is temperature, y is ln(FIR)) with a correlation coefficient of 0.998. The relative temperature sensitivity (S_r) of the film can be expressed by the following equation (Eq. 3):

$$S_r = \left|\frac{1}{\mathrm{FIR}} * \frac{\partial \mathrm{FIR}}{\partial T}\right| \times 100 = \frac{C * \exp\left(-\frac{\Delta E}{k_B T}\right)}{B + C * \exp\left(-\frac{\Delta E}{k_B T}\right)} \times \frac{\Delta E}{k_B T^2} \times 100\% \quad (3)$$

The maximal S_r value for the $CsPbBr_3$-KSF-PS film is 6.30% K^{-1} at 318 K, which is two times higher than that of $CsPbBr_3$-PS film (the S_r value for the $CsPbBr_3$-PS film is 2.61% K^{-1} at 318 K), and is much higher than most reported data (Table S1 in Supporting information). As shown in Fig. 2c, the resolution of the film is estimated to be 0.2 °C.

The high sensitivity of $CsPbBr_3$-KSF-PS film to temperature change also endows it with good potential for colorimetric temperature sensing. The PL color of the film (Fig. 2d) shows obvious change from green to yellowish brown then to red as the temperature increases from 30 °C to 70 °C, which can be readily recognized by naked eyes under an excitation of 365 nm UV light. The Commission International Ed'Eclairage 1931 (CIE 1931) diagram (Fig. 2e) clearly illustrates the change of PL color from green at 30 °C to yellow at 45 °C. The PL color turns to orange at 55 °C, then to red at higher temperature. In addition, the color transition of the film can be regulated by the mass ratio of $CsPbBr_3$:KSF, which is beneficial to the temperature sensing requirements in different situations. As discussed before, in Fig. 2e, apparent PL color change occurred at 45 °C (from green to yellow) and 55 °C (from yellow to red) when the mass ratio of $CsPbBr_3$:KSF was 3:8, which provides two visual signal for the detection system using one film. When the ratio of $CsPbBr_3$:KSF was 2:7 (Fig. S3 in Supporting information), apparent PL color change occurred at 40 °C (from green to yellow) and 50 °C (from yellow to red). Similarly, apparent PL color changed at different temperature can be achieved by controlling the mass ratio of $CsPbBr_3$:KSF equaled to 6:7 and 5:2. By calculation, the maximal S_r value for the $CsPbBr_3$-KSF-PS film is 10.31% K^{-1} at 318 K with the mass ratio of $CsPbBr_3$:KSF equaled to 5:2. The results demonstrate that the $CsPbBr_3$-KSF-PS film can meet the demand for the colorimetric temperature sensing in different scenes.

The thermal stability of the $CsPbBr_3$-KSF-PS sensing film was tested by heating up to a higher temperature and then cooling back to room temperature while monitoring the PL spectra. As shown in Fig. 3a, the film maintained acceptable thermal stability and repeatability during 6 heating-cooling cycles (from 30 °C to 70 °C), and still retained 95% of initial intensity when the temperature was back to room temperature. In addition, in the test of long-term stability for the $CsPbBr_3$-KSF-PS sensing film, the film was exposure to ambient air at room temperature for 3 months, and the fluorescence spectra at different temperature were collected (Fig. 3b). The FIR of the film remained its initial value basically, indicating no obvious degradation occurred.

In order to explore the sensing mechanism of the $CsPbBr_3$-KSF-PS film with the higher temperature sensitivity, the time-resolved PL spectra of the film at different temperatures were collected. With the increase of temperature, the PL lifetime of the sensing film decreased significantly (Fig. 4a), and the PL lifetime at 70 °C was less than 60% of that at 30 °C (Table S2 in Supporting

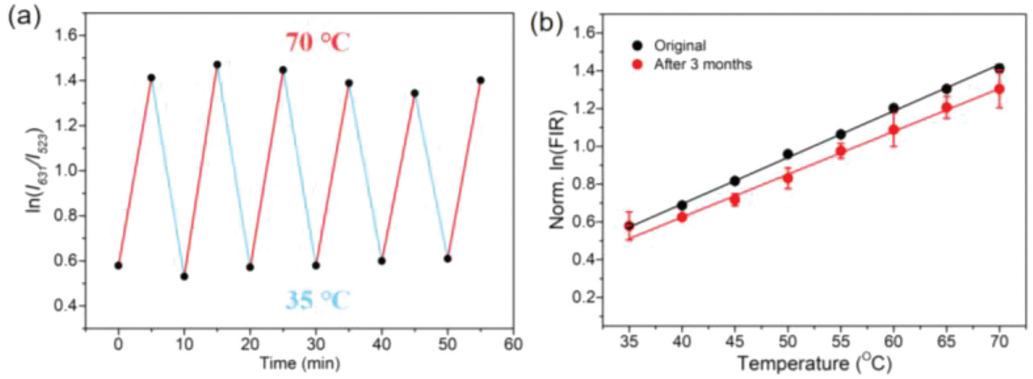

Fig. 3. (a) The thermal stability test of the film, the heating and cooling cycles are from 35 °C to 70 °C. (b) The linear relationship between the logarithm of FIR and the temperature of the film in its initial state and after three months of placement at different temperatures.

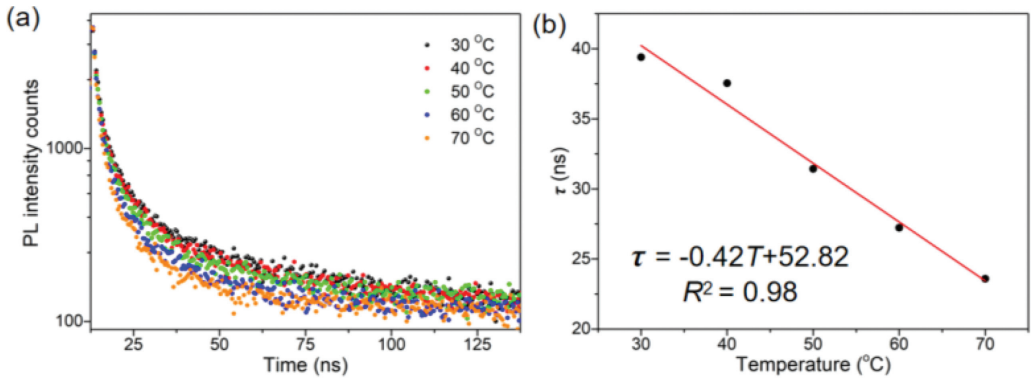

Fig. 4. (a) The fluorescence lifetime of the film at different temperatures. (b) The linear relationship between the lifetime and the temperature of the film.

information). There is a good linear relationship between PL lifetime and temperature (Fig. 4b), and the correlation coefficient is 0.98. The reduced PL lifetime indicates the increase of trapping which is consistent with the previous reports [26]. According to the previous reports, the reversible PL loss at elevated temperature is probably caused by halide vacancies related to thermal-assisted trapping. As the temperature increases, the optical phonon vibration frequency increases, and the carrier-phonon coupling is more likely to occur, which can be interpreted by the increase of the ratio of short-lived component τ_1 from 21.6% at 30 °C to 36.7% at 70 °C.

In summary, we successfully prepared a dual emission sensing film of $CsPbBr_3$ NCs and KSF encapsulated in polystyrene to construct a reversible visual temperature sensing system. The as-prepared $CsPbBr_3$-KSF-PS film shows a great temperature sensing performance in the temperature range from 30 °C to 70 °C with a relative temperature sensitivity (S_r) up to 10.31% $°C^{-1}$ at 45 °C and a temperature resolution of about 0.2 °C. The temperature change can be identified by the naked eye. The temperature discoloration point of the sensing film could be adjusted by changing the ratio of $CsPbBr_3$:KSF to adapt the different temperature sensing range, which provides an essential strategy for highly sensitive temperature sensing using $CsPbBr_3$ NCs in biological fermentation and other fields.

Declaration of competing interest

The authors declare that they have no known competing financial interests or personal relationships that could have appeared to influence the work reported in this paper.

Acknowledgments

The authors gratefully acknowledge the financial supports by the Shenzhen Science and Technology Project (No. JCYJ20180306172823786), and the National Natural Science Foundation of China (Nos. 21876141, NFFTBS-J1310024).

Supplementary materials

Supplementary material associated with this article can be found, in the online version, at doi:10.1016/j.cclet.2022.01.017.

References

[1] X. Zhu, J. Li, X. Qiu, et al., Nat. Commun. 9 (2018) 2176–2187.
[2] T. Bai, N. Gu, Small 12 (2016) 4590–4610.
[3] I.E. Kolesnikov, D.V. Mamonova, M.A. Kurochkin, E.Y. Kolesnikov, E. Lähderanta, J. Lumin. 231 (2021) 117828.
[4] M.G. Nikolić, Ž. Antić, S. Ćulubrk, J.M. Nedeljković, M.D. Dramićanin, Sens. Actuators B: Chem. 201 (2014) 46–50.
[5] L. Tong, X. Li, J. Zhang, et al., Opt. Express 25 (2017) 16047–16058.
[6] H. Zheng, B. Chen, H. Yu, et al., J. Colloid Interface Sci. 420 (2014) 27–34.
[7] H. Zheng, B. Chen, H. Yu, et al., Sens. Actuators B: Chem. 234 (2016) 286–293.
[8] S. Wang, J. Jiang, Y. Lu, et al., J. Lumin. 226 (2020) 117418.
[9] Y. Park, C. Koo, H.Y. Chen, A. Han, D.H. Son, Nanoscale 5 (2013) 4944–4950.
[10] Y. Zhou, D. Zhang, J. Zeng, N. Gan, J. Cuan, Talanta 181 (2018) 410–415.
[11] Q. Luo, H. Wang, X. Yin, L. Wang, Sci. China Mater. 62 (2019) 1065–1070.
[12] P.C. Tsai, C.P. Epperla, J.S. Huang, et al., Angew. Chem. Int. Ed. 56 (2017) 3025–3030.
[13] N. Rakov, S.A. Vieira, Q.P.S. Silva, G.S. Maciel, Sens. Actuators B: Chem. 209 (2015) 407–412.
[14] J. Liu, Y. Zhao, X. Li, et al., Cryst. Growth Des. 20 (2019) 454–459.
[15] X.D. Wang, X.H. Song, C.Y. He, et al., Anal. Chem. 83 (2011) 2434–2437.
[16] S. Xu, W. Ouyang, P. Xie, et al., Anal. Chem. 89 (2017) 1617–1623.
[17] C. Wang, T. Hu, T. Thomas, et al., Nanoscale 10 (2018) 21809–21817.

[18] J.S. Niezgoda, B.J. Foley, A.Z. Chen, J.J. Choi, ACS Energy Lett. 2 (2017) 1043–1049.
[19] Y. Wei, Z. Cheng, J. Lin, Chem. Soc. Rev. 48 (2019) 310–350.
[20] T.L. Doane, K.L. Ryan, L. Pathade, et al., ACS Nano 10 (2016) 5864–5872.
[21] X. Li, Y. Yu, J. Hong, et al., J. Lumin. 219 (2020) 116897.
[22] L. Protesescu, S. Yakunin, M.I. Bodnarchuk, et al., Nano Lett. 15 (2015) 3692–3696.
[23] A. Swarnkar, R. Chulliyil, V.K. Ravi, et al., Angew. Chem. Int. Ed. 54 (2015) 15424–15428.
[24] Q.A. Akkerman, V. D'Innocenzo, S. Accornero, et al., J. Am. Chem. Soc. 137 (2015) 10276–10281.
[25] Y. Wang, J. He, H. Chen, et al., Adv. Mater. 28 (2016) 10710–10717.
[26] B. Zhuang, Y. Liu, S. Yuan, et al., Nanoscale 11 (2019) 15010–15016.
[27] J. Guo, B. Zhou, C. Yang, Q. Dai, L. Kong, Adv. Funct. Mater. 29 (2019) 1902898.
[28] Y. Wang, J. He, H. Chen, et al., Adv. Mater. 28 (2016) 10710–10717.
[29] B.T. Diroll, G. Nedelcu, M.V. Kovalenko, et al., Adv. Funct. Mater. 27 (2017) 1606750.
[30] X. Li, Y. Wu, S. Zhang, et al., Adv. Funct. Mater. 26 (2016) 2435–2445.